Thermomechanical modelling of a blast furnace hearth

Jérôme Brulin, Alain Gasser, Amna Rekik, Eric Blond, Frédéric Roulet

Version of Record: https://www.sciencedirect.com/science/article/pii/S0950061822005190
Manuscript_7d84dbee959fc6ff0b10728cd5f46e31

Thermomechanical modelling of a blast furnace hearth

Jérôme Brulin[1], Alain Gasser[2,*], Amna Rekik[2], Eric Blond[2], Frédéric Roulet[1]

[1] *Saint-Gobain Research Provence, 550 avenue A. Jauffret, 84306 Cavaillon, France*
[2] *Univ. Orléans, Univ. Tours, INSA-CVL, LaMé, 8 rue L. de Vinci, 45072 Orléans, France*
[*] *Corresponding author*

jerome.brulin@saint-gobain.com, alain.gasser@univ-orleans.fr, amna.rekik@univ-orleans.fr, eric.blond@univ-orleans.fr, frederic.roulet@saint-gobain.com

Abstract
A blast furnace hearth is made of several refractory layers and materials. To improve its design and to determine the most sensitive zones, a thermomechanical finite element model was built. The material properties are temperature dependent. The carbon ramming mix, a compacting material which absorbs part of the thermal expansion, is represented by a modified Cam-Clay model. The masonries with mortar joints (in the bottom and in the ceramic cup) are replaced by an orthotropic material that has a behaviour equivalent to that of the masonries. Since failure can occur either in mortar joints or brick/mortar interfaces, different joint states are considered (according to the "open" or "closed" state of the joints in each direction). The interface strength, determined experimentally, was taken into account through a Mohr-Coulomb criterion. The equivalent material parameters were obtained, for each joint state, using a periodical homogenization method. The simulation was performed in two steps: first, computation of the thermal field, and second, computation of the displacements and stress fields. The comparison with experimental measurements on a real blast furnace showed that the model produces satisfactory results. The results also showed the importance of the initial ramming mix density and the influence of joint openings.

Keywords: blast furnace hearth, thermomechanical modelling, refractory masonry, periodical homogenization, joint opening criterion, finite element simulation.

Nomenclature

a	Size of the yield surface (modified Cam-Clay model)
c	Cohesion (Mohr-Coulomb model)
$\bar{\bar{C}}$	Stiffness matrix
C_{ijkl}	Components of the stiffness matrix
$\bar{\bar{E}}$	Second order macroscopic strain tensor
E_{kl}	Components of the macroscopic strain tensor
f	Yield function
f_t	Tensile strength
F	Associated flow rule (modified Cam-Clay model)
h	Heat transfer coefficient
$k(T)$	Thermal conduction (temperature dependent)
M	Slope of the critical state line (modified Cam-Clay model)
p	Hydrostatic pressure
p_c	Hydrostatic compression
q	Equivalent von Mises stress
$\vec{q}$	Heat flux density

T	Temperature
u_i	Displacement in direction i
w	Strain energy density
β	Constant modifying the shape of the cap (modified Cam-Clay model)
$\bar{\bar{\delta}}$	Second order identity tensor
$\bar{\bar{\varepsilon}}$	Second order strain tensor
ε_{ij}	Components of the strain tensor
λ	Lamé coefficient
μ	Lamé coefficient
ϕ	Internal angle of friction (Mohr-Coulomb model)
$\bar{\bar{\sigma}}$	Second order stress tensor
σ_{ij}	Components of the stress tensor
σ_n	Normal stress
$\bar{\bar{\Sigma}}$	Second order macroscopic stress tensor
Σ_{ij}	Components of the macroscopic stress tensor
τ	Shear stress

1. Introduction

Blast furnaces produce pig iron by reducing iron ore in integrated steel plants. The hearth is the part of the blast furnace located under the tuyere zone (Figure 1). It is the most critical part since a major incident in this part will have a major impact on all downstream activities and will lead to serious loss. In the Saint-Gobain design, the hearth is made of a steel shell (80 mm thick), a layer of porous carbon blocks (jointed without mortar), a bottom, a ceramic cup and a carbon ramming mix (90 mm thick) between the carbon block layer and the steel shell. The ceramic cup (Figure 2a) and the bottom (Figure 2b) are masonries with SiAlOn bonded corundum bricks and mortar joints (3.5 mm thick for the ceramic cup, 2 mm for the bottom). They protect the carbon blocks against the corrosion of gases and pig iron. They also decrease the temperature in these carbon blocks.

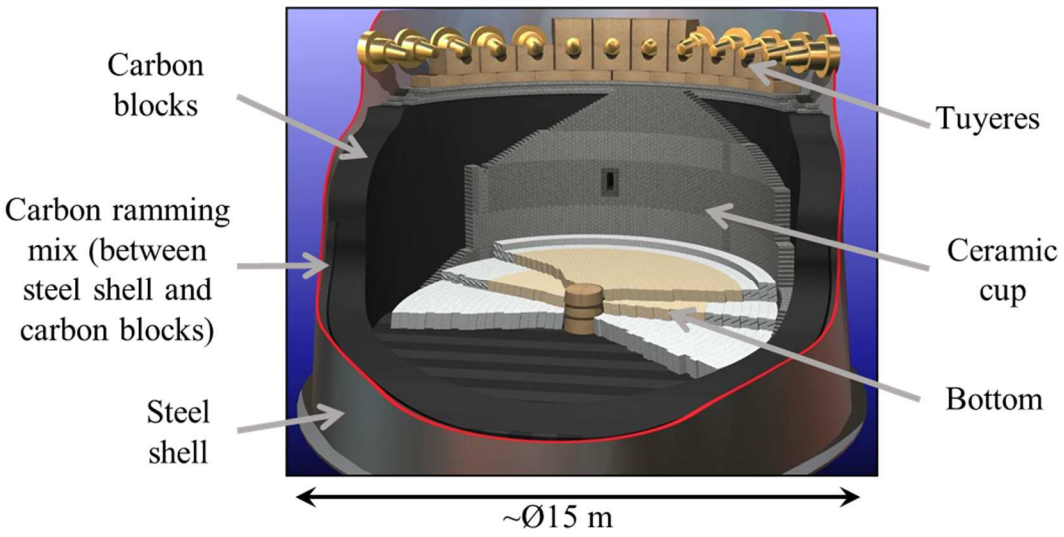

Figure 1: Blast furnace hearth.

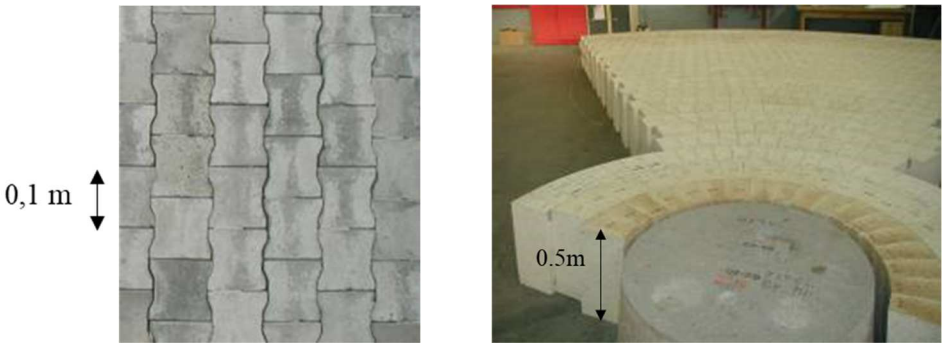

Figure 2: Ceramic cup (a) and bottom (b) masonries.

To optimize the design of the blast furnace hearth and increase its lifespan, a thermomechanical model can be used. It is worth noting that the temperature distribution in the blast furnace hearth is known thanks to several thermal modelling studies. For instance, Gdula et al. [1] built a 2D model in which the hearth was represented as concentric lining layers. These layers were divided into several regions where the temperatures are unknown. By solving the problem region after region, the unknown temperatures were determined. Kurpisz [2] extended this model to take into account the erosion of the carbon blocks. More recently, models using the finite element method were developed [3,4]. Concerning the thermomechanical computation (in which the thermal field is part of the loading), few models exist, and they propose some simplifications. For example, Gruber et al. [5], using a finite element software, modelled a slice of the hearth wall considering the dry joints but not the mortar joints of the masonries. The bottom was not modelled. Piret et al. [6] performed an axisymmetric simulation by finite elements. The model considered the “thick” joints (containing the ramming mix) and the contacts between the carbon blocks, but not the mortar joints of the bottom and ceramic cup (the behaviour of these two masonries comprising bricks and mortar was simplified as the behaviour of the bricks alone). There is therefore currently no model that considers all the joints in the masonries of a blast-furnace hearth. However, it is known that these joints play an important role in the structure behaviour, decreasing the stresses [7, 8].

The difficulty when considering a finite element model is to correctly represent the thermomechanical behaviour of the masonries with mortar joints. It is not possible to represent each brick and each joint because they are too numerous. The computational time will be too high, and problems of convergence would occur in the case of joint opening (corresponding to mortar failure or brick/mortar interface failure) due to contact management.

To overcome these problems, it is proposed here to replace the masonry by a homogeneous material that has a behaviour equivalent to the set of bricks and joints, using a periodic homogenization technique. This approach was already used for refractory masonries with dry joints [9] and has to be adapted to mortar joints (contrary to dry joints for which it is necessary to use a joint closure criterion, a joint opening criterion must be defined here).

To determine the properties of the homogeneous equivalent material of the different masonries of the blast furnace hearth, it is necessary to know beforehand and to model the mechanical behaviour of the different materials (bricks and mortars) of the masonries from room temperature (R.T.) up to 1450°C. It is also necessary to determine the brick/mortar interface strength to identify the parameters of the joint opening criterion.

Another important material is the carbon ramming mix located between the steel shell and the carbon blocks. Its high-compacting behaviour is very specific. It can absorb the deformation

of the parts submitted to high thermal loads. Its behaviour is represented with a modified Cam-Clay model.
In the following, the material properties (associated to the different material behaviour laws) are presented first. The periodic homogenization procedure will then be described, with its application to the ceramic cup and the bottom. Finally, the finite element model of a blast furnace hearth will be presented in two steps: the thermal and the mechanical models (thermo-mechanical uncoupling is assumed). The results are compared to measurements performed on a real blast-furnace.

2. Characterisation of materials behaviours

The blast-furnace hearth is made of several materials (Figure 3). The bottom is made of a castable at the centre, and three layers: carbon blocks, a masonry made of alumina bricks (mullite) and alumina cement A, and a masonry made of chamotte bricks and alumina cement A.
The wall is made of a steel shell, a ramming mix, a carbon block layer, a castable and a ceramic cup (masonry with SiAlOn bonded corundum bricks and alumina cement B).

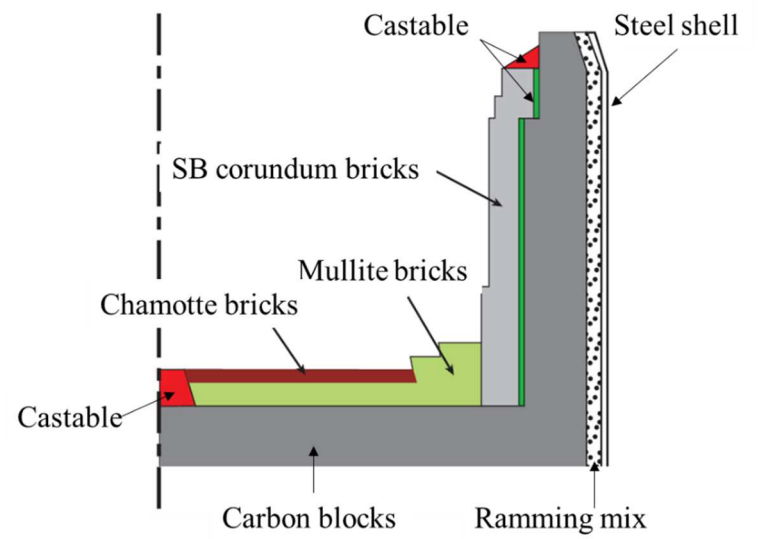

Figure 3: Materials of the blast furnace hearth.

2.1 Material properties

The behaviour of the steel is isotropic linear elastic (Young's modulus E=210 GPa, Poisson's ratio ν=0.3) at the stress level (less than its elastic limit) found in the steel shell of a blast furnace, and temperature independent (the steel shell temperature is close to room temperature). All other materials have a linear behaviour until 1000°C. Only the materials in contact with the pig iron are submitted to a temperature higher than 1000°C and present a visco-plastic behaviour. In this first approach, for simplification, this nonlinear behaviour at high temperature (over 1000°C) was not considered. So, carbon block, brick, mortar and castable behaviours are assumed to be as isotropic linear elastic, but temperature dependent.
Young's moduli were determined using uniaxial compression tests at different temperatures. The tests were performed on cylinders with a height of 50mm, an external diameter of 50mm and an internal diameter of 12mm. In the case of mortars (cements A and B), the specimen

was made of 3 layers of mortar and 4 washers of brick (the same brick material as the one associated to the mortar in the blast-furnace), see Figure 4. The Young's moduli obtained versus temperature are given in Table 1.

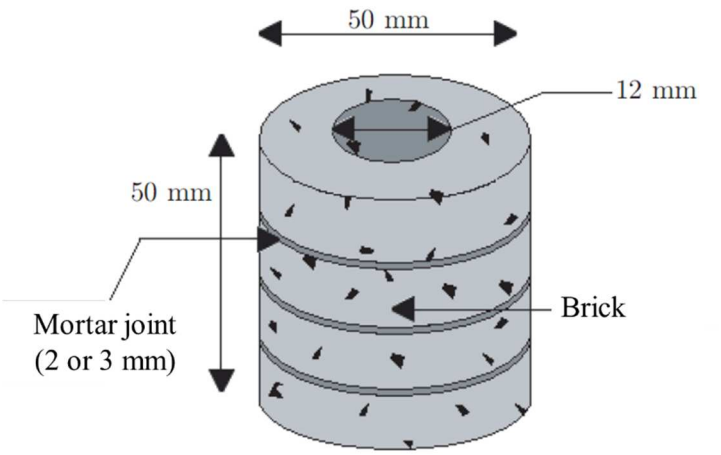

Figure 4: Specimen to determine the mortar behaviour.

	20°C	500°C	900°C	1200°C	1450°C
Carbon	10.2	10			
Cement A	0.48		0.29	0.05	0.02
Cement B	1.24		1.22	0.16	2.78
Castable		14.3		13.5	3.6
SB corundum	13.8		8.3	34	11
Mullite	18.6		23.6	11.9	2.5
Chamotte	8.4			6.4	0.6

Table 1: Young's moduli (GPa) of the different materials constituting the blast-furnace hearth versus temperature (since some materials are exposed only to high temperatures, and others to "lower" temperatures, depending on their location in the lining thickness, they were not tested at all temperatures between 20°C and 1450°C).

2.2 Brick/mortar interface

The opening of joints corresponds to the failure of the brick/mortar interface or the mortar. The shear strength of the brick/mortar interface typically depends on the normal stress applied to the interface. This friction type behaviour can be described by the Mohr-Coulomb yield function:

$$f(\tau, \sigma_n, \Phi) = |\tau| - c + \sigma_n tan\Phi \qquad (1)$$

where τ is the shear stress, σ_n is the normal stress (negative in compression), c is the cohesion of the material and ϕ is the internal angle of friction (Figure 5). Determination of cohesion

and the internal friction angle requires the measurements of normal and shear stresses until failure.
A tensile cut-off corresponding to tensile failure is added to complete the interface failure criterion. It is defined by:

$$f(\sigma_n, f_t) = \sigma_n - f_t \qquad (2)$$

where f_t is the tensile strength (Figure 5). In a tensile test of a quasi-brittle material, carried out under controlled displacement, the tensile strength corresponds to the peak of the stress-displacement curve.

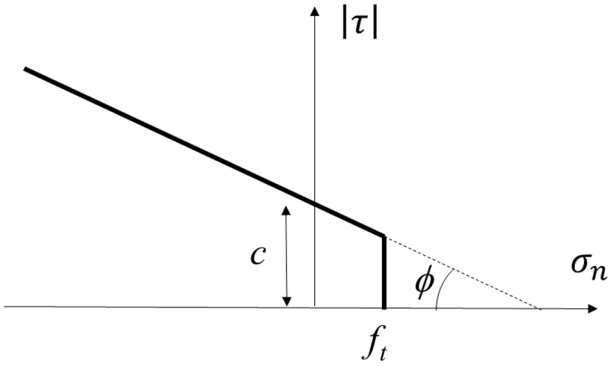

Figure 5: Brick/mortar interface failure criterion [10].

The parameter identification of these two criteria is extensively described in Brulin *et al.* [10]. The parameters of the Mohr-Coulomb failure criterion were obtained using slant shear tests. The specimens, made of two bricks and a mortar joint inclined with respect to the horizontal line (Figure 6), were submitted to a normal compression load. Depending on the angle of inclination, the ratio between normal and shear stresses is different. With tests on specimens with three different angles, it is then possible to determine the cohesion c and the internal angle of friction ϕ.

(a) (b)

Figure 6: Failed specimens (of section 35x35 mm^2) with different angles of inclination after a slant shear test: (a) interface failure, (b) mortar failure.

The tensile strength f_t was obtained with a specific tensile test [10] performed on a brick/mortar specimen (Figure 7) fixed on the testing machine with nickel-chromium alloy wires, flexible enough to ensure the alignment of the loading "chain".

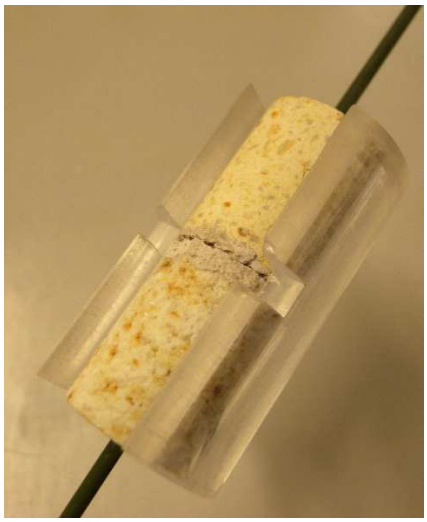

Figure 7: Brick/mortar specimen for tension test and its mould [10].

Table 2 shows the values of cohesion, friction angles and tensile strengths determined at different temperatures for the interface between either mullite bricks and cement A or corundum bricks and cement B. The values are almost constant until 900°C, but a marked decrease in the interface strength is observed at 1200°C and 1450°C.

	Mullite/cement A			SB corundum /cement B		
Temperature	c (MPa)	ϕ (°)	f_t (MPa)	c (MPa)	ϕ (°)	f_t (MPa)
R.T.	3.44	35	1.29	2.82	53	1.96
900°C	3.29	52	1.03	4.74	47	1.89
1200°C			0.18			0.21
1450°C	0.12	48		0.04	56	

Table 2: Cohesions, friction angles and tensile strengths identified at different temperatures for the interfaces mullite bricks/cement A, and corundum bricks/cement B (tensile strengths are limited to 1200°C due to wire creep during tensile tests for higher temperatures).

2.3 Ramming mix

A ramming mix made of graphite (80%) and coal tar (20%) is located between the carbon blocks and the steel shell. It is porous, so it is easy to compact: plastic deformations appear during compaction, that lead to volume change and stiffness increase. It absorbs the thermal expansion of the different refractory linings, and it protects the steel shell. In the blast furnace, its temperature is between 20°C and 80°C.
This type of behaviour with hardening can be modelled by a Modified Cam-Clay model [11] which is an extension of the theory developed by Roscoe and Burland [12] for geotechnical materials. This model is based on a yield surface given by the associated flow rule:

$$F = \frac{1}{\beta^2}\left(\frac{p}{a} - 1\right)^2 + \left(\frac{q}{Ma}\right)^2 - 1 = 0 \quad (3)$$

where p is the hydrostatic pressure, q the equivalent von Mises stress, M the slope of the critical state line, a the size of the yield surface and β a constant which can modify the shape of the cap (see Figure 8).

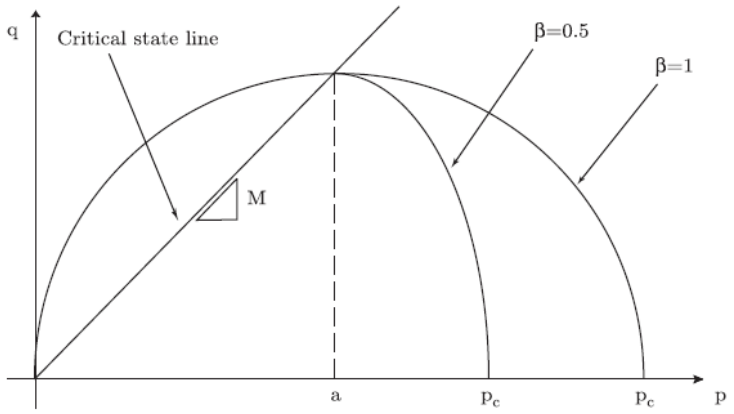

Figure 8: Yield surface and critical state line of the Modified Cam-Clay model [13].

For a hydrostatic compression p_c, the yield stress is given by:

$$p_c = a(1 + \beta) \qquad (4)$$

The hardening behaviour is characterized by the growth of the yield surface size defined by the evolution of a [13].
To determine the parameters of this model, triaxial tests and die compaction tests were performed between 20°C and 80°C. The description of these tests, the results obtained, the parameter identification, and the model validation are extensively presented in Brulin et al. [13]. Table 3 gives the values of the yield surface parameters for three different temperatures.

Temperature (°C)	20	50	80
M	1.18	1.1	1.1
β	1	0.56	0.21

Table 3: Parameters of the yield surface of the modified Cam-Clay model for the ramming mix.

3. Masonry modelling

In masonries, joints between bricks play an important role. In a blast furnace hearth, they are made of mortars that have a stiffness much lower than that of bricks. They allow the decrease of the stresses in the masonry because they counterbalance the deformation due to thermal expansion. So, it is necessary to take them into account during a numerical simulation. In a finite element model of a real industrial structure (with thousands of bricks), it is not possible to model each brick and each joint (due to problems of convergence and very high computing time cost). The idea here is to replace the masonry by a homogeneous material that has a

behaviour equivalent to that of the masonry. The properties of this equivalent material were determined using a periodic homogenization technique [14-16].

3.1 Periodic homogenization step

The studied masonries present a periodical structure. Therefore, to perform the homogenization, the Representative Elementary Volume (REV) corresponds to the elementary cell that is reproduced periodically.
The equivalent material has an orthotropic elastic behaviour because:

- the masonries present three orthogonal planes of symmetry,
- the number of joints is different in the two directions of a wall,
- joints can be open (failed mortar or brick/mortar interface) in one direction and closed (safe mortar and brick/mortar interface) in the other direction.

In that case, the stiffness matrix $\bar{\bar{C}}$ (that links macroscopic stresses Σ_{ij} to macroscopic strains E_{kl}) has nine independent components (C_{ijkl}):

$$\begin{pmatrix} \Sigma_{11} \\ \Sigma_{22} \\ \Sigma_{33} \\ \Sigma_{23} \\ \Sigma_{13} \\ \Sigma_{12} \end{pmatrix} = \begin{pmatrix} \mathrm{C}_{1111} & \mathrm{C}_{1122} & \mathrm{C}_{1133} & 0 & 0 & 0 \\ \mathrm{C}_{1122} & \mathrm{C}_{2222} & \mathrm{C}_{2233} & 0 & 0 & 0 \\ \mathrm{C}_{1133} & \mathrm{C}_{2233} & \mathrm{C}_{3333} & 0 & 0 & 0 \\ 0 & 0 & 0 & \mathrm{C}_{2323} & 0 & 0 \\ 0 & 0 & 0 & 0 & \mathrm{C}_{1313} & 0 \\ 0 & 0 & 0 & 0 & 0 & \mathrm{C}_{1212} \end{pmatrix} \begin{pmatrix} \mathrm{E}_{11} \\ \mathrm{E}_{22} \\ \mathrm{E}_{33} \\ 2\mathrm{E}_{23} \\ 2\mathrm{E}_{13} \\ 2\mathrm{E}_{12} \end{pmatrix} \qquad (5)$$

To identify these nine components, nine different loads (three uniaxial tension or compression loads, three biaxial tensile or compression loads and three shear loads) were simulated by finite elements on the REV. These loads correspond to homogeneous macroscopic strains represented by the second order macroscopic strain tensor $\bar{\bar{E}}$:

$$\bar{\bar{E}} = \begin{pmatrix} E_{11} & E_{12} & E_{13} \\ E_{12} & E_{22} & E_{23} \\ E_{13} & E_{23} & E_{33} \end{pmatrix} \qquad (6)$$

The strain energy density w of the REV is written as:

$$w = \frac{1}{2}(\mathrm{C}_{1111}E_{11}^2 + \mathrm{C}_{2222}E_{22}^2 + \mathrm{C}_{3333}E_{33}^2) + \mathrm{C}_{1122}E_{11}E_{22} + \mathrm{C}_{1133}E_{11}E_{33} + \mathrm{C}_{2233}E_{22}E_{33} + 2(\mathrm{C}_{1212}E_{12}^2 + \mathrm{C}_{1313}E_{13}^2 + \mathrm{C}_{2323}E_{23}^2) \qquad (7)$$

For example, considering a uniaxial tension load in direction 1, the homogeneous macroscopic strain tensor is:

$$\bar{\bar{E}} = \begin{pmatrix} E_{11} & 0 & 0 \\ 0 & 0 & 0 \\ 0 & 0 & 0 \end{pmatrix} \qquad (8)$$

So, from equations 7 and 8, the strain energy density is equal to:

$$w = \frac{1}{2}\mathrm{C}_{1111}E_{11}^2 \qquad (9)$$

This strain energy density is obtained by a finite element computation on the calculation domain (the REV or one part of it if it shows some geometrical symmetries). Loads and boundary conditions are presented on Figure 9 for the uniaxial tensile load in direction 3 in the case of a 3D REV with two planes of symmetry ((1,3) and (2,3)). Notice that the boundary conditions consider the periodicity and symmetry properties.

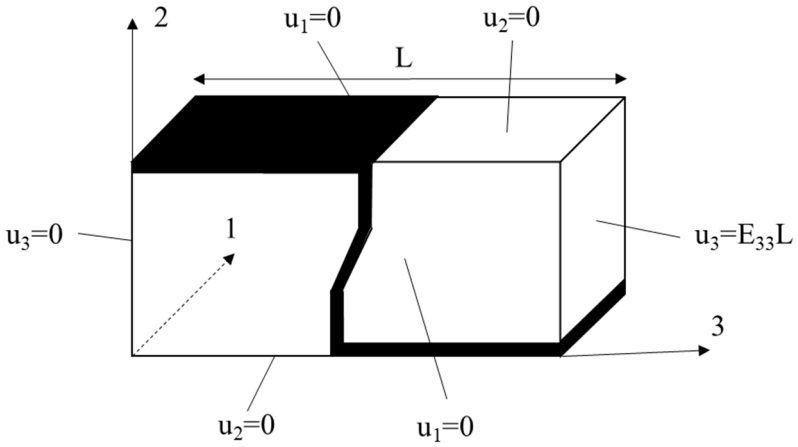

Figure 9: Calculation domain (see Figure 10), load (displacement u_3) and boundary conditions (displacements u_i in direction i) for a uniaxial tensile load in direction 3.

The calculated strain energy allows with Equation 8 the determination of the stiffness component C_{1111}:

$$C_{1111} = \frac{2w}{E_{11}^2} \qquad (10)$$

The eight other stiffness components are determined in a similar manner with the eight other loads.
In the case of a 2D axisymmetric modelling in plane 12 (which is the case here, see section 4), shear stresses in planes 13 and 23 are zero. So, the stiffness components C_{1313} and C_{2323} are not necessary, and hence are not computed.
During loading, the mortar or the interface between brick and mortar can fail. This corresponds to a joint opening. In a masonry with different joint directions, joints can be open in some directions and closed in others. This corresponds to different "joint states" [16]. The number of joint states depends on the number of different joint directions. For example, in a masonry with two joint directions (bed and head joints), four states are considered [9].
In each state, the masonry will have a different behaviour. It is therefore necessary to perform the periodic homogenization for each state to determine the parameters of the equivalent material. For each state, it is assumed that the equivalent material has an elastic linear behaviour, but due to the possible state changes during the masonry loading, the masonry will have globally a nonlinear behaviour.
The last step consists in formulating a criterion that defines the condition of joint opening (to go from one state to another). This corresponds to the failure of the brick/mortar interface or the mortar in shear or in tension as defined in subsection 2.2.
The equivalent material behaviour law of the masonry (for the different joint states and with the brick/mortar interface failure criterion) is introduced in a finite element software using a user material subroutine.

3.2 Homogenization of the ceramic cup masonry

The ceramic cup is a cylindrical wall made of alumina (SB corundum) interlocking bricks with mortar (Figure 9). Due to the large diameter of this cylinder (almost 15m), it is possible to consider this masonry as flat to determine the parameters of the equivalent material in Cartesian space. The elementary periodic 3D cell has two planes of symmetry, so the computational domain, made of bricks and mortar, is one quarter of this periodic cell (Figure 10).

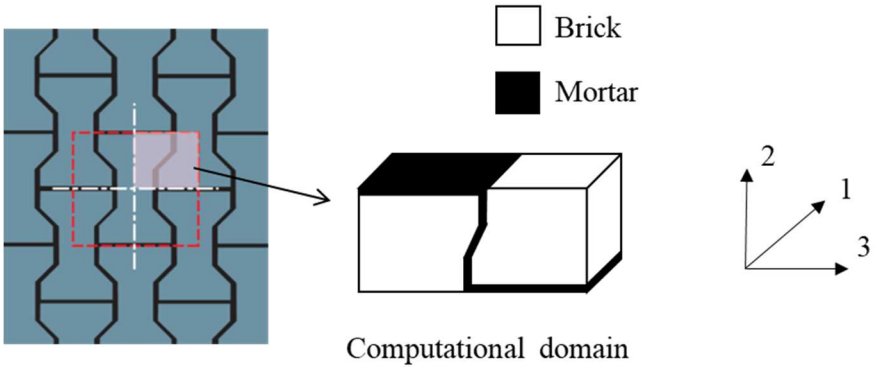

Figure 10: Ceramic cup masonry and domain of FE computation (one quarter of the periodic cell).

For this masonry, bed and head joints are present. So four joint states (combination of open or closed bed and head joints) must be considered (Figure 11). An equivalent orthotropic behaviour is determined for each of these states under several temperatures. For example, Table 4 gives the stiffness components at 1450°C. It can be noticed that joint failures cause some stiffness components to be reduced to zero.

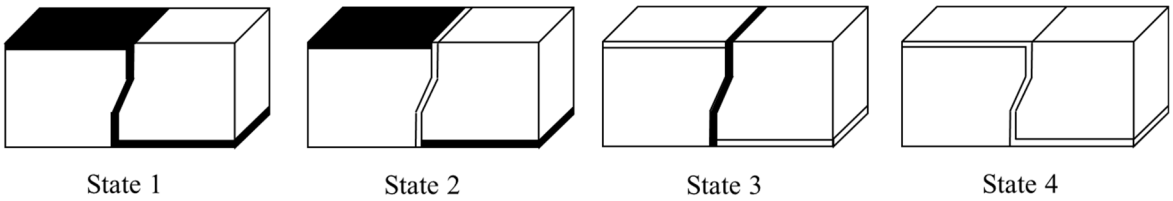

Figure 11: Joint states for the ceramic cup masonry (failed/open joints are in white).

	State 1	State 2	State 3	State 4
C_{1111} (MPa)	11335	10712	10783	10330
C_{2222} (MPa)	10764	9975	851	527
C_{3333} (MPa)	10835	0	10341	0
C_{1122} (MPa)	2563	1935	222	0
C_{1133} (MPa)	2584	0	2063	0
C_{2233} (MPa)	2463	0	255	0
C_{1212} (MPa)	4069	4036	1093	0

Table 4: Stiffness components of ceramic cup masonry equivalent material at 1450°C.

The joint opening criteria (which make it possible to go from one joint state to another) are presented on Figure 12. They are a combination of tension failure (tensile cut-off) and shear failure (Mohr-Coulomb). The values of f_t, c and ϕ are given in Table 2 for different temperatures. For example, to go from state 1 to state 2, the vertical joints can open by tension in direction 3 or by shear in the plane (1,2). In that case, the vertical joint is assumed to be totally broken (open) in the REV.

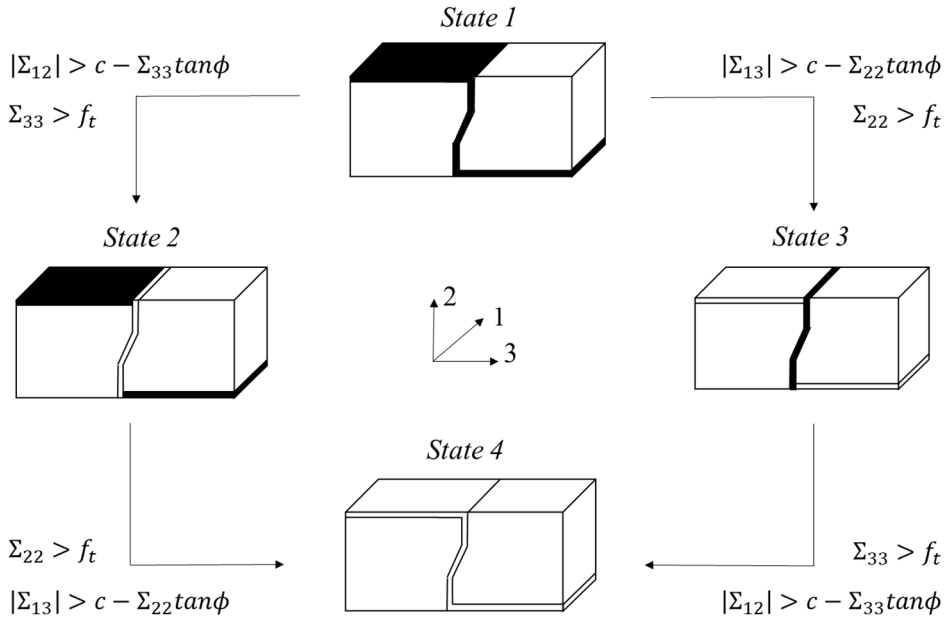

Figure 12: Joint opening criteria for the ceramic cup masonry.

3.3 Homogenization of the bottom masonry

The bottom is made of two masonry layers (one with chamotte bricks, the other with mullite bricks) with a radial design (Figure 13). Each layer includes twenty crowns of bricks. Each crown is made of two types of bricks with different dimensions (the maximum difference in dimension between the smallest and the largest brick is 10%). Furthermore, due to the change of radius between the crowns, the shape of the bricks evolves from inside to outside crowns. Consequently, the radial masonry is not periodic.

To simplify the modelling, it was considered that each crown is periodic (that means only along the orthoradial or circumferential direction), using a "mean" brick with mean dimensions. In that case, the periodic cell consists of one brick (and some mortar joints). Due to symmetry, the computational domain is half of a brick (Figure 13). An equivalent material was determined for each crown. It was observed that the differences between the coefficients obtained for the different crowns are less than 10%. It was then considered that the radial masonry can be modelled by a homogeneous material that behaves like crown number 10 which is the "mean" crown. Note that the orthotropic behaviour is written in a cylindrical coordinate system.

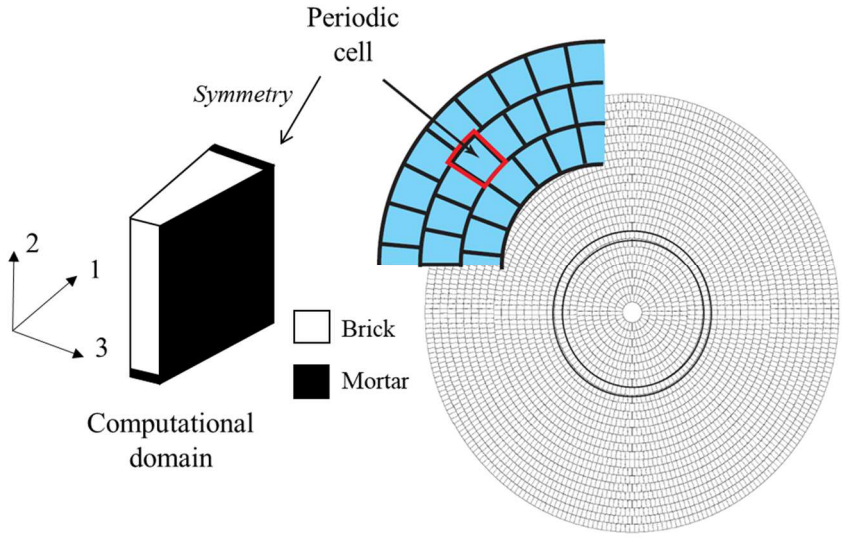

Figure 13: Bottom masonry and computational domain.

For this masonry, three directions of joints are present (see Figure 13): horizontal joints located in the (1,3) plane, vertical joints in the radial direction and vertical joints in the circumferential direction. So, eight joint states (combination of open or closed joints in the three directions) must be considered (Figure 14). An equivalent orthotropic behaviour was determined for each of these states and for several temperatures. For example, Table 5 gives the values obtained at 1450°C for the bottom masonry made of chamotte bricks. As mentioned previously, in the case of a 2D axisymmetric modelling in plane 12, shear stresses in planes 13 and 23 are zero. So, the stiffness components C_{1313} and C_{2323} are not necessary.

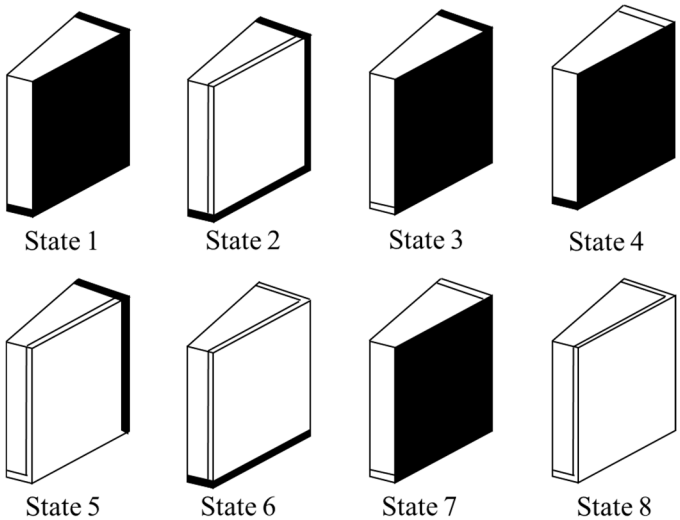

Figure 14: Joint states for the bottom masonry (failed/open joints are in white).

	State 1	State 2	State 3	State 4	State 5	State 6	State 7	State 8
C_{1111}	522	508	508	0	497	0	0	0
C_{2222}	556	540	0	540	0	527	0	0
C_{3333}	461	0	455	447	0	0	439	0
C_{1122}	109	94	0	0	0	0	0	0
C_{1133}	91	0	83	0	0	0	0	0
C_{2233}	97	0	0	87	0	0	0	0
C_{1212}	197	196	0	0	0	0	0	0

Table 5: Stiffness components (in MPa) of bottom masonry (made of chamotte bricks) equivalent material at 1450°C.

In the same manner as for the ceramic cup, joint opening/failure criteria were defined between the eight joint states (joints can fail in tension or in shear), see Figure 15.

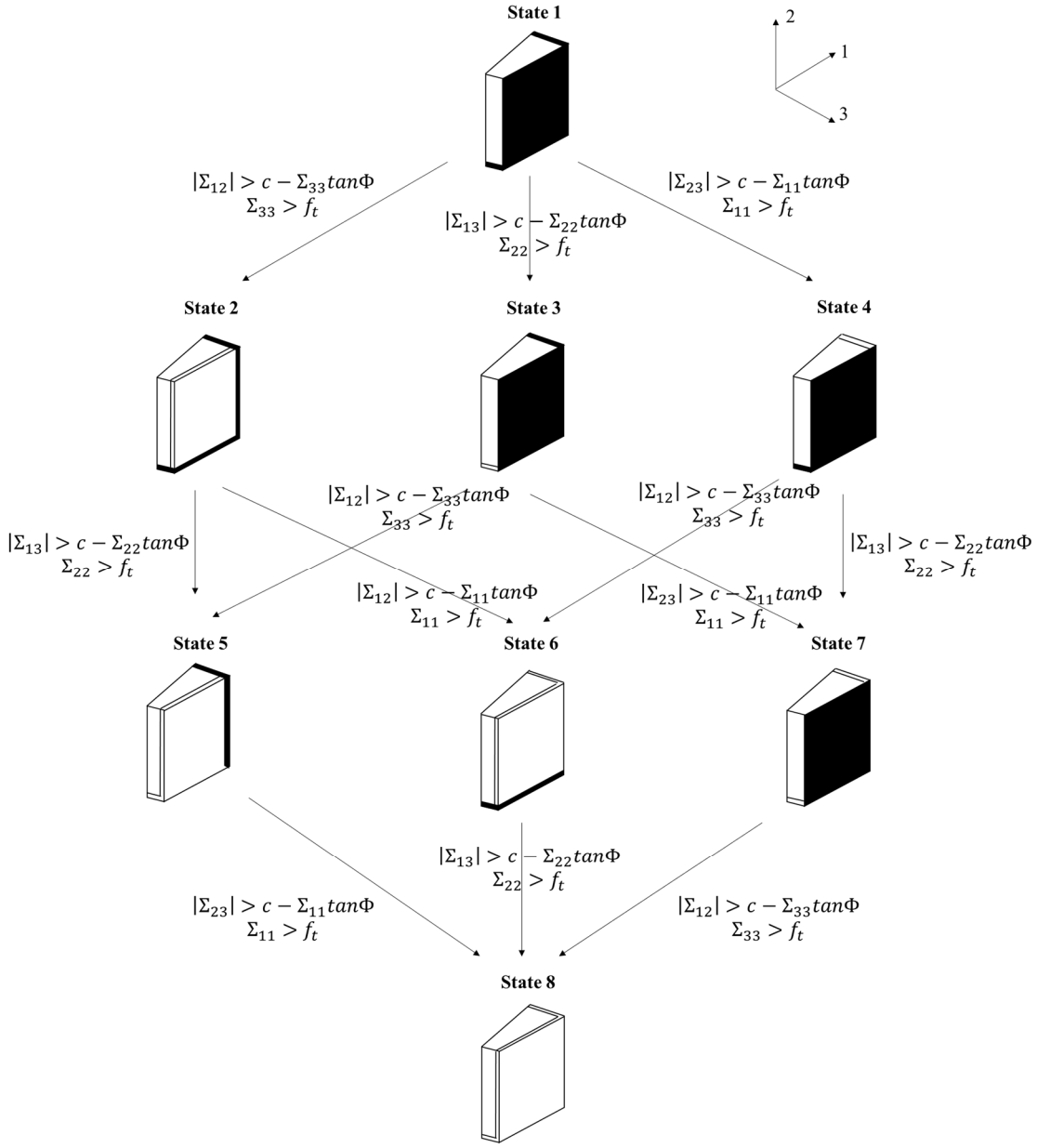

Figure 15: Joint opening criteria for the bottom.

4. Blast-furnace hearth modelling

A thermomechanical finite element model of the blast furnace hearth was built using Abaqus software. Due to the shape of this structure, it is possible, in a first approach, to use a 2D axisymmetric model to reduce computational time. The structure was meshed with axisymmetric quadrilateral elements with four nodes. The mesh (Figure 16) is made up of 14300 elements and 16000 nodes.
A weak thermo-mechanical coupling was considered. First, the thermal field was computed considering the different thermal transfers (material conduction and convection with the surrounding environment). Secondly, this thermal field was used as load (in addition to the other mechanical loads) in a mechanical computation to determine displacements and stresses. As the mesh is the same for the two simulations, the node temperatures obtained in the thermal simulation were directly applied on the same nodes of the mechanical simulation.

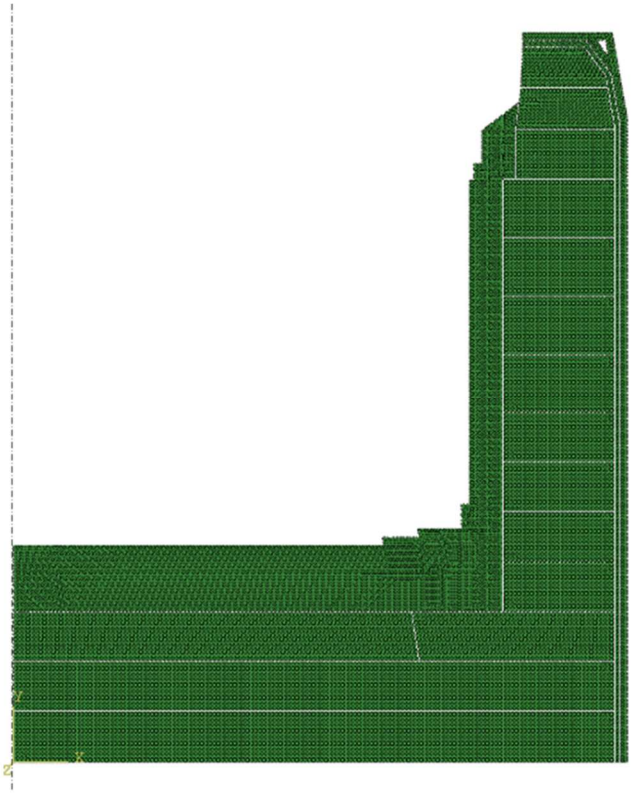

Figure 16: Mesh of the blast furnace hearth.

Each carbon block is represented, with contact with its neighbours. To perform the mechanical computation with many contacts, an explicit approach was used.
The bottom and ceramic cup masonries were replaced by their temperature dependent equivalent materials. The equivalent material behaviour laws were introduced in Abaqus using a subroutine (VUMAT).

4.1 Thermal modelling

Since the steel shell is cooled during operation, a temperature of 30°C was imposed on the outer steel shell face. Cooling tubes (with water) are also located under the carbon blocks in the blast furnace hearth bottom. They are embedded in the ramming mix which is not modelled in the bottom. Consequently, the heat transfer (between the water and the carbon

blocks) by conductivity in the ramming mix was replaced by an equivalent heat transfer by convection (that assumes a perfect heat transfer between water and tubes and between tubes and ramming mix) directly between water (at a temperature of 30°) and carbon blocks (Figure 17). The heat transfer coefficient (126 $Wm^{-2}K^{-1}$) was obtained by dividing the ramming mix conductivity (13.9 $Wm^{-1}K^{-1}$) by the ramming mix thickness (110 mm).
The heat exchanges between the pig iron and the hearth masonries (bottom and wall) were modelled by a convection, with a heat transfer coefficient of 150 $Wm^{-2}K^{-1}$ (this value is the one used by the design offices responsible for the thermal calculations) and a pig iron temperature of 1450°C (Figure 17).
All thermal contacts are assumed to be perfect (the total heat flux goes through the interface). The initial temperature is 20°C. The steady state thermal field is then determined by solving the heat equation (time independent and without an internal heat source):

$$div\vec{q} = 0 \qquad (11)$$

with $\vec{q}$ the heat flux density given by the Fourier law:

$$\vec{q} = -k(T)\overrightarrow{gradT} \qquad (12)$$

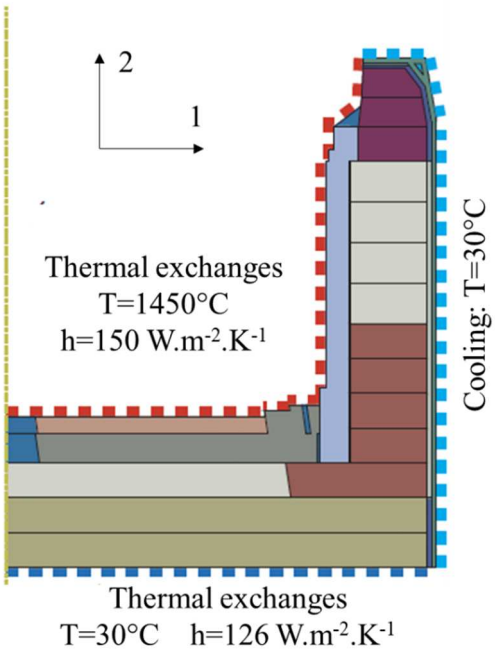

Figure 17: Thermal axisymmetric modelling of the blast-furnace hearth.

4.2 Mechanical modelling

For the mechanical modelling, the contact with friction was defined between the different layers and between the carbon blocks using a Coulomb contact law. The friction coefficients were measured at room temperature using an inclined plane [18]. They are equal to the tangent of the angle of inclination corresponding to the beginning of relative sliding between the two materials. The friction coefficients obtained were: carbon/carbon (0.25), castable/carbon (0.7), steel/ramming mix (0.2) and carbon/ramming mix (0.3).

The masonries were replaced by their corresponding equivalent material (section 3). The Modified Cam-Clay model was used for the ramming mix.
The hearth is laid on the ground, so vertical displacement of the bottom surface of the hearth is equal to zero (Figure 18). The axisymmetry condition results in a zero-horizontal displacement on the vertical axisymmetric axis.
The loads are as follows (Figure 18):

- The thermal field obtained by the thermal model
- The gravity
- The hydrostatic pressure (0.4 MPa at the bottom level, zero at the top of the hearth) on the internal faces (bottom and wall) due to pig iron (density of 6400kg/m^3), slag (2700kg/m^3) and coke (450 kg/m^3) floating on the liquid iron. The maximum value (0.4 MPa) was obtained by multiplying the density by the gravity acceleration and the liquid height
- The gas pressure (0.5 MPa) applied on the steel shell (the refractory materials being porous, the gas can go through them and reach the steel shell)
- The pressure (15 MPa) at the top of the wall corresponding to the load of the top part of the blast furnace. This load represents the weight of the top part, but also the vertical loads applied to this part (gas pressure and load due to friction between the steel shell and the burden mass during its descent).

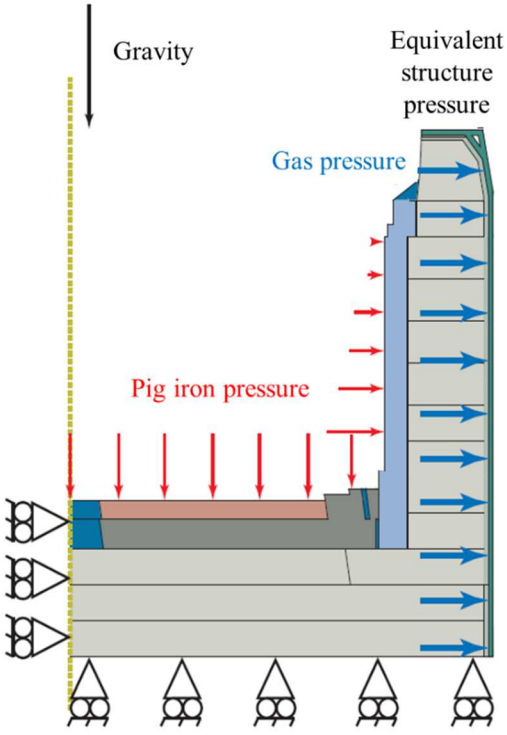

Figure 18: Mechanical loads and boundary conditions.

5. Results and discussion

The temperature field obtained is presented in Figure 19. The influence of the ceramic cup can be observed. It plays the role of insulation decreasing the temperature in the carbon blocks (maximum of 500°C).

Temperatures were compared to measurements obtained by Saint-Gobain with 17 thermocouples located in the carbon blocks (12 in the wall and 5 in the bottom) in a real blast furnace (Figure 19). These measurements correspond to 24-hour average values, one month after the first heating (the steady state of the blast furnace was reached). Table 6 shows a good agreement between measured and computed temperature values (the maximum relative difference is 16%) considering the precision of measurements and thermocouple location. Therefore, the temperature field is validated and can be used for the mechanical simulation.

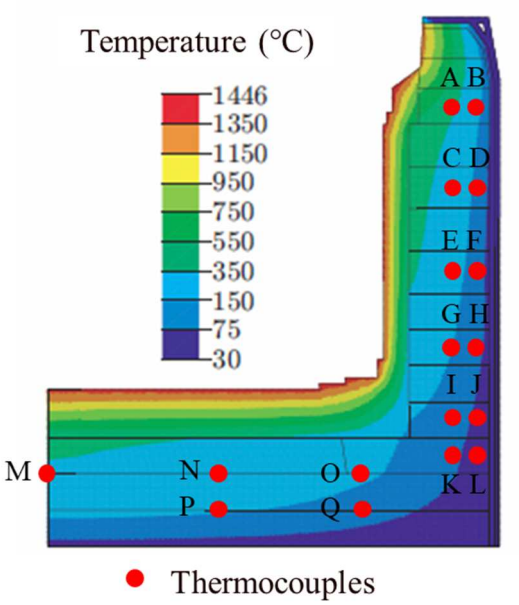

Figure 19: Computed thermal field and location of the thermocouples.

Thermocouple	Measured temperature (°C)	Computed temperature (°C)	Difference (%)
A	212	231	9
B	139	127	9
C	165	153	7
D	102	93	9
E	132	124	6
F	81	78	4
G	94	102	9
H	69	73	6
I	64	74	16
J	51	56	10
K	58	63	9
L	48	50	4
M	300	311	4
N	260	264	2
O	147	170	16
P	141	157	11
Q	91	105	15

Table 6: Comparison between measured and computed temperatures.

To observe the influence of joint opening in the masonry, but also the ramming mix initial relative density (RD), four mechanical models were tested:

- No joint openings and RD=80% (corresponding to a density of 1450 kg/m^3, a value generally observed in the blast furnace)
- No joint openings and RD=92% (corresponding to a density of 1680 kg/m^3, which is the recommended theoretical value)
- Joint openings and RD=80%
- Joint openings and RD=92%.

Figure 20 shows the joint openings in the bottom and ceramic cup masonries. It can be observed that most openings concern the bottom part of the bottom masonry with vertical joint opening (state 2). On the other hand, no joint openings are present at the surface in contact with pig iron, showing that the blast furnace hearth is watertight to molten iron.

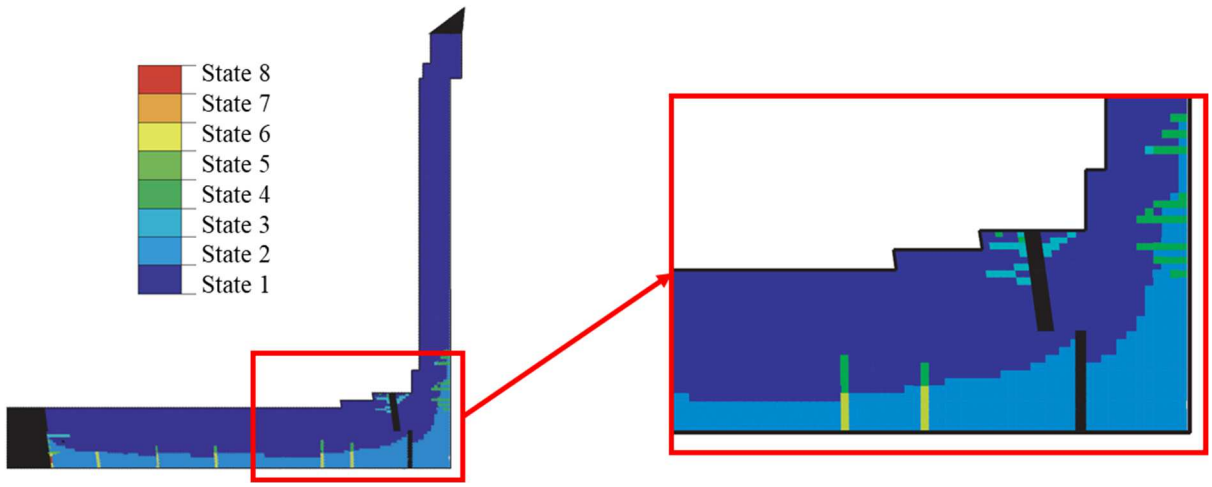

Figure 20: Joint openings in masonries, bottom and ceramic cup (black zones are made of castable).

Figure 21 shows the evolution of the von Mises stresses in the steel shell along a vertical line for the four models. The maximum values are in the bottom area, due to the bottom expansion.
The possible joint openings allow a decrease in the stresses, in particular in the bottom area (due to joint openings in the bottom, see Figure 20). Likewise, the decrease in the ramming mix relative density leads to a decrease in these stresses due to a higher deformation capacity. This influence is lower in the case of joint openings, however: the stresses are the same until a height of 3 m, and only differ for a higher height. This can be explained by the fact that almost all joint openings occur in the bottom, a phenomenon that will decrease the stresses considerably (maximum stresses divided by 2).
The elastic limit of the steel shell is 250 MPa. For safety reasons, however, the maximum admissible von Mises stress must not exceed 100 MPa after a few weeks of operation (the stresses can be higher during the first heating but subsequently decrease due to relaxation). The model that considers the joint openings, with an initial ramming mix relative density of 80%, gives a maximum von Mises stress just over this limit (Figure 21).

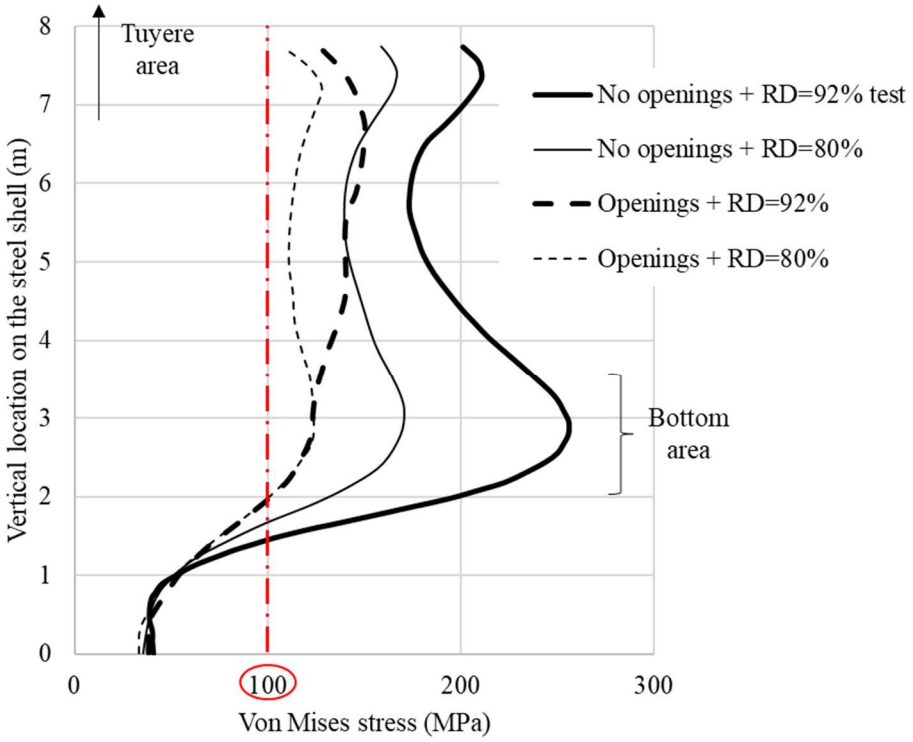

Figure 21: Von Mises stresses in the steel shell.

Figure 22 reports the evolution of the radial displacement of the steel shell along a vertical line for the four models. As for von Mises stresses, the joint openings and the decrease in the ramming mix relative density decrease the radial displacements, in particular in the bottom area.

A value of 5 mm of the radial displacement at a height of 5 m was measured on the real blast furnace. This value corresponds to the model that considers the joint openings, with an initial ramming mix relative density of 80%. This relative density value is quite close to the real value. It is difficult to determine it precisely during the construction of the blast furnace due to manual compaction. However, some measurements on real blast furnaces suggest that an 80% relative density is the most probable installation state.

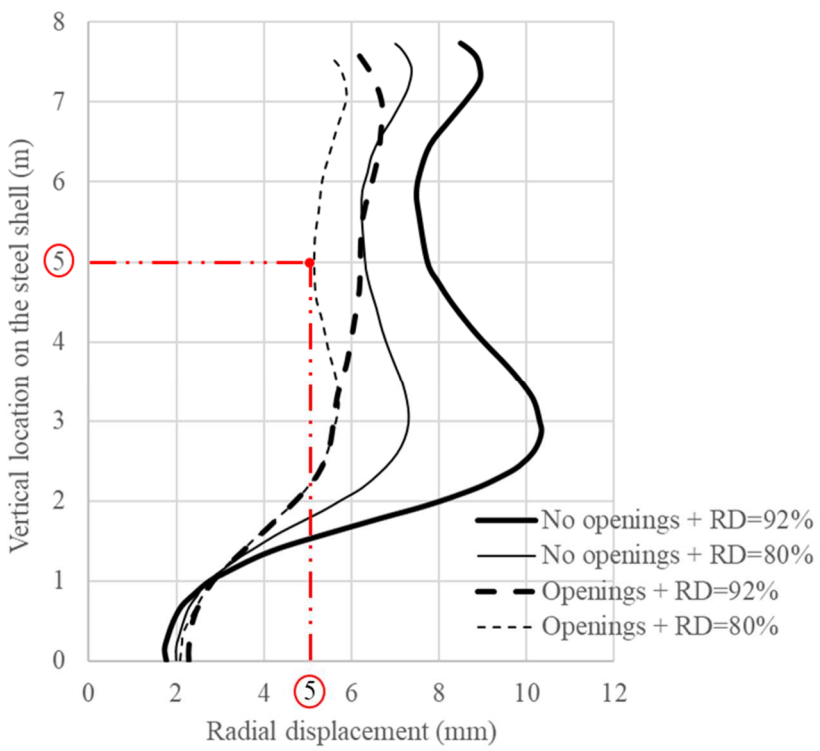

Figure 22: Radial displacement of the steel shell as a function of the height.

Two strain gages were glued on the steel shell at a height of 3 m. They measure the axial ($\varepsilon_{zz} = 450.10^{-6}$) and circumferential ($\varepsilon_{\theta\theta} = 50.10^{-6}$) strains. Assuming that the steel shell is in a plane stress state and that radial, orthoradial and axial directions correspond to the principal stress directions, the stress tensor can be written in the cylindrical coordinate system (r, θ, z) as follows:

$$\bar{\bar{\sigma}} = \begin{pmatrix} 0 & 0 & 0 \\ 0 & \sigma_{\theta\theta} & 0 \\ 0 & 0 & \sigma_{zz} \end{pmatrix} \qquad (11)$$

In that case, the strain tensor is written as follows:

$$\bar{\bar{\varepsilon}} = \begin{pmatrix} \varepsilon_{rr} & 0 & 0 \\ 0 & \varepsilon_{\theta\theta} & 0 \\ 0 & 0 & \varepsilon_{zz} \end{pmatrix} \qquad (12)$$

The linear elastic isotropic behaviour law is:

$$\bar{\bar{\sigma}} = 2\mu\bar{\bar{\varepsilon}} + \lambda(Tr\bar{\bar{\varepsilon}})\bar{\bar{\delta}} \qquad (13)$$

where λ and μ are the Lamé coefficients, and $\bar{\bar{\delta}}$ the second order identity tensor. One deduces:

$$\varepsilon_{rr} = -\frac{\lambda}{(2\mu+\lambda)}(\varepsilon_{\theta\theta} + \varepsilon_{zz}) \qquad (14)$$

$$\sigma_{\theta\theta} = (2\mu + \lambda)\varepsilon_{\theta\theta} + \lambda(\varepsilon_{rr} + \varepsilon_{zz}) \qquad (15)$$

$$\sigma_{zz} = (2\mu + \lambda)\varepsilon_{zz} + \lambda(\varepsilon_{rr} + \varepsilon_{\theta\theta}) \qquad (16)$$

The equivalent von Mises stress is equal to:

$$q = \sqrt{\frac{1}{2}\left[\sigma_{\theta\theta}^2 + \sigma_{zz}^2 + (\sigma_{\theta\theta} - \sigma_{zz})^2\right]} \qquad (17)$$

A value of 94 MPa is obtained for the Von Mises stress (which is less than the steel elastic limit). Table 7 shows the comparison of the strains given by the four models and the measured strains. The two models with joint openings give the same values as already observed in Figure 21 at a height of 3 m (the ramming mix initial relative density has little influence on strains in the case of joint openings).
It is observed again that the model with joint openings and the lower ramming mix density gives the results closest to those of the measurements. But the computed values are still too high. This is due to the fact that the model does not take into account the visco-plastic behaviour of the refractory materials at high temperature [18]. This nonlinear behaviour is the origin of creep and relaxation in refractory structures which decreases the stresses over time. This phenomenon plays an important role and therefore will be considered in further investigations [19].

	Axial strain (10^{-6})	Circumferential strain (10^{-6})	Von Mises equivalent stress (MPa)
Measurement	450	50	94
No openings + RD=92%	1130	230	240
No openings + RD=80%	800	180	171
Openings + RD=92%	650	130	137
Openings + RD=80%	650	130	137

Table 7: Comparison of strains between measurements (by strain gages) and the four models.

6. Conclusions

An axisymmetric thermomechanical model of a blast furnace hearth was built by coupling the homogenization technique and the finite element method. It considers the material temperature dependent behaviour and the specific ramming mix compacting behaviour. The masonries with mortar joints were replaced by homogeneous orthotropic materials whose behaviour approximates that of the masonries. The brick/mortar interface strengths were measured, enabling a joint opening criterion to be identified which was then used to determine the joint state (open or closed) during the loading.
The results obtained were compared to some measurements obtained on a real blast furnace: temperatures from 17 thermocouples, steel shell radial displacement and strains. The comparison shows that the numerical model reproduces these measurements accurately. The simulations have shown that joint opening and ramming mix play an important role, decreasing the stresses. The initial relative density of the ramming mix must not be too high, otherwise the stresses in the steel shell will exceed the maximum allowed stress.
This model will be of help for blast-furnace design as it allows the modification of some parameters (geometry, ramming mix initial density, brick size and shape, joint thickness, material properties, lining thickness) to observe their influence, to minimize the stresses and to improve the blast-furnace lifespan.
To improve the model, the next step is to consider the nonlinear behaviour of bricks at high temperature. Over 1000°C, refractory materials have an elastic-visco-plastic behaviour which

causes creep and relaxation of the refractory linings. These phenomena decrease the stresses inside the blast furnace hearth over time.
Another improvement is to consider the wear of the linings (decrease in the thickness) due to corrosion by gases and pig iron. A simple approach is to consider a reduced lining (bottom and ceramic cup) thickness in the computation. A more precise approach, but still under development [20], is to associate a thermochemical model to the proposed thermomechanical model.

Acknowledgements

This work was supported by Saint-Gobain Research Provence.

References

[1] S. Gdula, R. Biaeecki, K. Kurpisz, A. Nowak, A. Sucheta, Mathematical model of steady state heat transfer in blast furnace hearth and bottom, Transactions ISIJ, 25 (1985) 380–385.

[2] K. Kurpisz, A method for determining steady state temperature distribution within blast furnace hearth lining by measuring temperature at selected points, Transactions ISIJ, 28 (1988) 926–929.

[3] L. F. Verdeja, R. González, A. Ordóñez, Using FEM to determine temperature distribution in a blast furnace crucible, J. of the Miner. Met. and Mater. Soc., 52 (2000) 74–77.

[4] S. Mehrotra, Y. Nand, Heat balance model to predict salamender penetration and temperature profiles in the sub-hearth of an iron blast furnace, ISIJ Int., 33 (1993) 938-846.

[5] D. Gruber, K. Andreev, H. Harmuth, FEM simulation of the thermomechanical behaviour of the refractory lining of a blast furnace, J. of Mater. Process. Technol., 155-156 (2004) 1539–1543.

[6] J. Piret, J. Menéndez Arias, M. Franken, P. Blumenfeld, Study of behaviour of cement and mass joint used in aggregates of steel industry, Sollac, Technical report, 2004.

[7] A. Gasser, K. Terny-Rebeyrotte, P. Boisse, Modelling of joint effects on refractory lining behaviour, J. of Mater.: Des. and Applications, 218 (2004) 19–28.

[8] A. Gasser, A. Rekik, E. Blond, K. Andreev, Comparison of different designs of bottom linings with dry joints, Proceedings of UNITECR'11, Kyoto (Japan), 2011.

[9] T.M.H. Nguyen, E. Blond, A. Gasser, T. Prietl, Mechanical homogenisation of masonry wall without mortar; Eur. J. of Mech. - A/Solids, 28 (2009) 535–544.

[10] J. Brulin, E. Blond, E. de Bilbao, A. Rekik, M. Landreau, A. Gasser, Y. Colleville, Methodology for brick/mortar interface strength characterization at high temperature, Constr. and Build. Mater., 265 (2020).

[11] Abaqus Standard Reference Manuals, version 6.7., Simulia, Providence, RI, USA, 2007.

[12] K.H. Roscoe, J.B. Burland, On the generalized stress-strain behaviour of 'wet' clay; Cambridge University Press, Eng. Plast., 1968, pp. 535-609.

[13] J. Brulin, A. Rekik, L. Josserand, E. Blond, A. Gasser, F. Roulet, Characterization and modelling of a carbon ramming mix used in high-temperature industry, Int. J. of Solids and Struct., 48 (2011) 854-864.

[14] M. Bornert, T. Bretheau, P. Gilormini, Homogenization in Mechanics of Materials, ISTE Publishing Company, 2006.

[15] A. Anthoine, Derivation of the in-plane elastic characteristics of masonry through homogenization theory, Int. J. of Solids and Struct., 32 (1995) 137–163.

[16] R. Luciano, E. Sacco, Homogenization technique and damage model for old masonry material, Int. J. of Solids and Struct., 34 (1997) 3191-3208.

[17] K. Terny-Rebeyrote, Analyse expérimentale et numérique des structures réfractorisées avec prise en compte des joints, PhD thesis of University of Orléans, 2004 (in French).

[18] L. Teixeira, S. Samadi, J. Gillibert, S. Jin, T. Sayet, D. Gruber, E. Blond, Experimental investigation of the tension and compression creep behavior of alumina-spinel refractories at high temperatures, Ceramics, 3 (2020) 372-383.

[19] ATHOR (Advanced THermomechanical multi-scale mOdelling Refractory linings), Marie Skłodowska-Curie Actions Innovative Training Networks of the European Commission, 764987 Grant (https://www.etn-athor.eu/).

[20] E. Blond, A. K. Nguyen, E. de Bilbao, T. Sayet, A. Batakis, Thermo-chemo-mechanical modeling of refractory behavior in service: Key points and new development, Appl. Ceram. Technol., 14 (2020) 1693-1700.